Article

Theoretical Analysis of the Catalytic Hydrolysis Mechanism of HCN over Cu-ZSM-5

Yankun Zhang, Fenji Li, Cuicui Yang, Guojian Peng, Guowei Wang and Futing Xia *

Key Laboratory of Resource Clean Conversion in Ethnic Regions, Education Department of Yunnan,
Yunnan Minzu University, Kunming 650500, China; zhangyankun0402@163.com (Y.Z.); lifenji2022@163.com (F.L.);
yangcc0718@163.com (C.Y.); pgj159357@163.com (G.P.); 18687014092@163.com (G.W.)
***** Correspondence: xiafuting@163.com; Tel.: +1-831-4382-129

Abstract: HCN catalytic hydrolysis mechanism over Cu-ZSM-5 was investigated based on the density functional theory (DFT) with 6-31++g (d, p) basis set. Five paths (A, B, C, D, and E) were designed. For path A and path B, the first step is the nucleophilic attack of water molecule. Next, the hydrogen atom of H_2O is transferred to the nitrogen atom first for path A, while in path B, the hydrogen atom of the HCN is first transferred to the nitrogen atom. In path C, HCN isomerizes to HNC initially, and the remaining steps are similar to that of path A. The H atom of HCN shifts to Cu-ZSM-5 initially in path D, and the H atom is transferred to N atom subsequently. The last step is the attack on water molecule. The first step for path E is similar to that of path D. The next step is the attack on water molecule, in which the H atom of water molecule shifts to N atom, and the H on Cu-ZSM-5 shifts to the N atom. Meanwhile, the H atom of oxygen atom is transferred to the N atom. The results show that path C is the most favorable path, with the lowest free energy barrier (35.45 kcal/mol). The results indicate that the Cu-ZSM-5 strongly reduces the energy barrier of HCN and isomerizes to HNC, making it an effective catalyst for HCN hydrolysis.

Keywords: HCN; catalytic hydrolysis; density functional theory; Gibbs free energy barrier; Cu-ZSM-5

1. Introduction

HCN is an "unconventional" toxic pollutant found in high amounts in industrial waste gas, such as coke gas [1], yellow phosphoric tail gas [2], sealed calcium carbide furnace tail gas [3], and processes that release NO_x [4,5]. HCN is very hazardous [6] and comprehensive emission standards for atmospheric pollutants (GB 16297-1996) report that the maximum non-toxic emission quality of HCN is 0.3 mg/m^3. Therefore, it is important to explore methods for removal of HCN from tail gas.

Several approaches for removal of HCN such as liquid absorption-catalytic oxidation (which has been banned), adsorption method [2,7,8], catalytic combustion method and gas-solid catalytic oxidation, and catalytic hydrolysis method have been reported [9–11]. Adsorption isa common method; however, it requires significantly high operation tempera-ture and results in secondary pollution. Catalytic combustion and the catalytic oxidation method require expensive catalysts and high reaction temperature thus limiting indus-trial application. On the other hand, catalytic hydrolysis caneffectively take place at low temperatures, and the products which include NH_3 and CO have low toxicity [12].

Several studies have explored the catalytic hydrolysis of HCN in the gas phase. Marsh et al., investigated the catalytic hydrolysis of HCN on Al_2O_3, and reported that it can be converted into NH_3 under 400 °C in the non-oxygen waste gas [13]. In addition, 78% conversion efficiency of HCN in water and oxygen was achieved over zeolitecoated with H-ferrierite [14]. In 2009, Kröcher et al., reported that Fe-ZSM-5 and Cu-ZSM-5 have excellent catalyticactivity for hydrolysis of HCN [10]. HCN is effectively converted to ammonia at temperatures above 300 °C on Fe-ZSM-5, and the converted HCN efficacy of Cu-ZSM-5 is higher than Fe-ZSM-5. Recent studies founded that Mn/TiO_2-Al_2O_3 for HCN

removal showed excellent HCN removal efficiency [15]. However, detailed analysis for the hydrolysis process of HCN and the possible catalytic mechanisms are unclear.

Density functional theory (DFT) is a promising technology for further understanding the mechanism of HCN catalytic hydrolysis due to toxicity of HCN, complexity of HCN hydrolysis experiments, and the high operating cost. DFT provides details on the complicated reaction mechanism, such as energy barriers, reaction routes, and the main structures. Extensive theoretical research have focused on the removal of HCN recently. Jensen et al., explored the HCN hydrolysis reaction with theoretical method, and reported that the main adsorption form of reactants was by O$\cdots$H adsorption interaction [16]. The B3LYP and MP2 methods have given different results for the addition of HCN or HNC to methanimine with formamidine. At B3LYP level, a lower intermediate with aminoacetonitrile has been located [17]. It has been [18] found that the addition of three water molecules giving rise to a ring reaction significantly favors isomerization. DFT calculations were carried out on the graphitic carbon nitride (g-C_3N_4) with the addition of transition metals (including Ni, Pd, and Pt) for adsorption of HCN gas. The results showed that Pt-embedded g-C_3N_4 was a suitable candidate for removing HCN gas. Song et al., reported that formation of the complex (HCN-H_2O) was an exothermic process [19,20]. Cu-ZSM-5 is an effective catalyst for hydrolysis of HCN; however, the catalytic process and reaction mechanism have not been fully explored. Therefore, there is a need to further explore the detailed reaction mechanisms of hydrolysis of HCN by Cu-ZSM-5. This study explores the mechanism of toxic HCN hydrolysis on Cu-ZSM-5 using theoretical calculations. Findings from this study provides useful information for removing HCN gas.

ZSM-5 with different unique pore structure, good shape selective catalytic activity, goodperformance, and high thermal stability are widely used in the field of catalysis (Figure 1). The cluster and periodic system of Fe-ZSM-5 had negligible differences by the density functional theory (DFT) calculations [21]. Zhang et al., explored adsorption of N_2O on transition ion exchange ZSM-5 using DFT [22]. Analysis showed that ZSM-5 was an effective auxiliary tool for N_2O removal. The exchangeable Fe^{2+} ions embedded ZSM-5 zeolite own excellent stability as shown by DFT analysis [23]. Czekaj et al. [24] investigated the adsorption and desorption of isocyanic acid over Fe-ZSM-5, and reported that isocyanic acid was in molecular form present over Fe-ZSM-5. These findings imply that ZSM-5 modeling is a feasible catalyst.
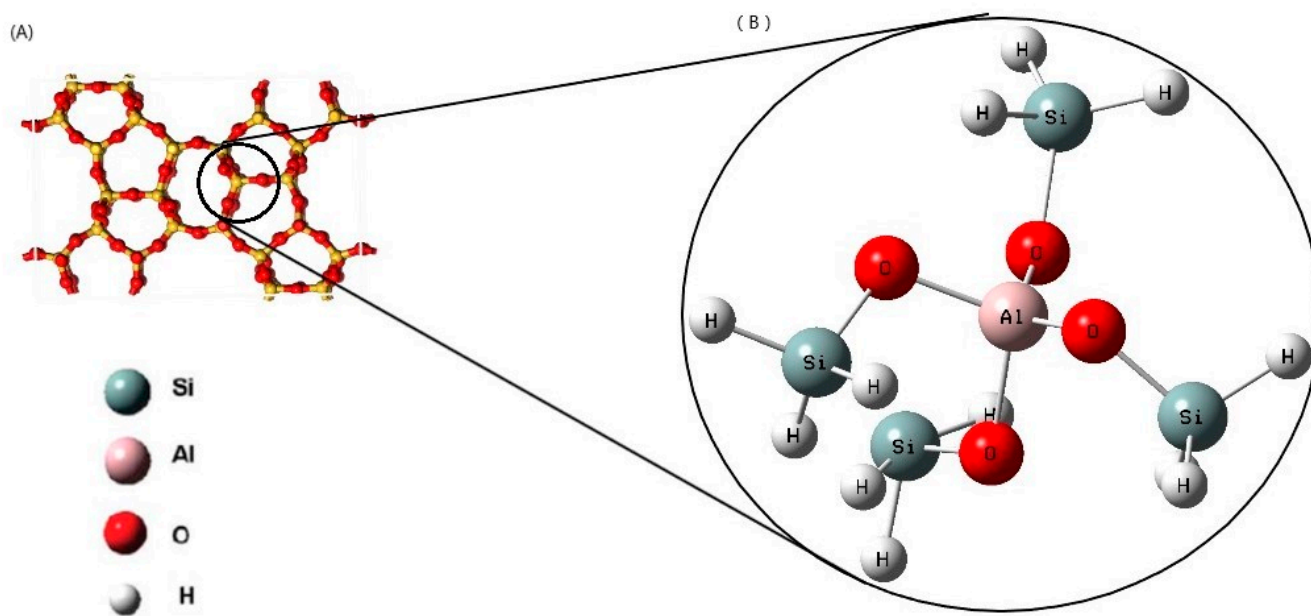

Figure 1. (**A**) ZSM-5 zeolite (**B**) optimized geometries for 5T ZSM-5 cluster.

In our previous work [25], we explored direct hydrolysis of HCN using second-order Møller–Plesset (MP2) theory with basis set 6-31++G (d,p). In the current study, catalytic hydrolysis of HCN over Cu-ZSM5 is explored by B3LYP method, to explore the effect of addition of Cu-ZSM5 catalyst on the five reaction paths.

2. Computational Details

All calculations were performed using Gaussian 03 package [26]. B3LYP/6-31++g (d,p) basis set was employed in the molecular geometries of the reactant complexes (RC), transition states (TS), intermediates (INT), and product complexes (PC). As to the element of Cu, its core electrons were represented by LANL2DZ effective core potential. B3LYP was characterized by relatively low cost and high accuracy information, therefore, it was used for theoretical calculations [27–29]. Zero-point energy (ZPE) [28] correction was considered in the reaction, and all energy, enthalpy correction, and Gibbs free energy corrections were based on the frequency calculation. Intrinsic reaction coordinates (IRC) calculations [29] were performed for each transition state to verify that all of the transition states were connected to the reactants and products.

3. Results and Discussion

In this study, catalytic hydrolysis of HCN over Cu-ZSM5 is explored by B3LYP method, to explore the effect of addition of Cu-ZSM5 catalyst on the five reaction paths. The optimized Cu/ZSM-5 stable configuration is shown in the Figure 2. The scheme of five reaction paths is shown in Figure 3, the main structure features of HCN hydrolysis with Cu-ZSM-5 are shown in Figures 4–8. Tables 1–5 list the relative energies with respect to the reactant complex. Zero energycorresponds to the separate reactants. Shapes of the Gibbs free energy profiles have been presented. For all hydrolysis paths, Cu-RC corresponds to reactant complexes; Cu-TS corresponds to transition states; Cu-INT corresponds to intermediates; and Cu-PC corresponds to product complexes.

3.1. Path A

The distance between HCN and H_2O decreases gradually. Figure 4 shows the reactant complexes for path A.In Cu-RC1, a C–H⋯O–type H–bond is formed, with an H1–O bond distance of 1.8138 Å. The distance between the H_2 and N atom is 4.6026 Å, and the distance between C and O atom is 2.9098 Å. In the Cu-TS1, the distance between C atom and O atom decreases to1.5575 Å, the distance between H_2 and N atom is reduced to 1.4721 Å compared with Cu-RC1. The O–H_2 atomic distance is 0.9655 Å in Cu-RC1, whereas it is 1.1793 Å in Cu-TS1. This vibrationrepresents the processes of both the broken O-H_2 bond and the formation of C=O and H_2–N bond. Moreover, Cu-TS1 has one imaginary frequency of -1673.44 icm^{-1}. Cu-INT1 is formed through Cu-TS1, which features as the broken O–H_2bond. The H_2–N bond and the C=O bond are effectively formed for effective transfer of H3 atom to the N atom of HCN, the position of H3 is twisted, thus getting closer to the N atom during conversion of Cu-INT1 to Cu-TS2. The energy barrier and only imaginary frequency of Cu-TS2 are 2.76 kcal/mol and -29.59 icm^{-1}. For Cu-TS2, the bond lengths of all bonds are very close to Cu-INT1. The distance between H_2 and O atom is reduced to 0.9710 Å compared with Cu-TS2. Cu-INT2 is formed in this step through Cu-TS2 with a H3–O–C–N dihedral angel (DA)of 0.5499° andthe free energy barrier $\Delta G^{\neq}$ for Cu-TS2 is 2.76 kcal/mol. In the subsequent steps, H3 initially shifts to the N atom, then H1 transfers and one rotational transition state Cu-TS3 emerges before the step of H3 transfer. The imaginary frequency of Cu-TS3 is-29.43 icm^{-1}, and all bond lengths from the Cu-TS2 to Cu-TS3 does not show significant changes. The distance between the H3 atom and N atom is 2.4750 Å in Cu-TS3, and the free energy barrier (0.01 kcal/mol) for this process is relatively low. After the transition state, Cu-TS3, Cu-INT3 is formed with a Gibbs free energy of 9.31 kcal/mol. The structure of Cu-INT3 is basically unchanged comparedto the Cu-TS3. In the next step, the H3–O bond is broken, and this change causes the next transition state Cu-TS4 to be formed thoughCu-INT3. The vibrational mode of the single

imaginary frequency of Cu-TS4 is -1864.48 icm^{-1}. This frequencyshows that the O atom of H$_2$O connects to the Cu atom of Cu-ZSM-5 forming Cu–O bond. In addition, the H3 atom of the water is transferred from the N atom of the HCN, and the length of the H3–O bond is increased to 1.2769 Å, whereas the distance between H3 atom and N atom decreases to 1.3683 Å. As a result, the four-membered transition state is overcome. Concomitantly, Cu-INT4 is formed through Cu-TS4 corresponding to a free energy of -14.44 kcal/mol, and the H3–N and H3–O bonds are formed and broken, respectively. The length of the H3–N bond is 1.0114Å, whereas the distance between H3 atom and O atom increases to 2.5074Å.
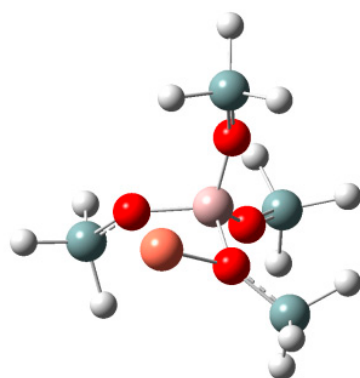

Figure 2. The model of Cu-ZSM-5.

Figure 3. The scheme of five reaction paths.

The last step is transfer of the proton (H1) from the carbon atom to the N atom of HCN. First, a three-membered transition state, Cu-TS5 is formed with a single imaginary frequency (-1920.46 icm^{-1}). The vibrational mode shows that the distance between H1 atom and N atom became smaller and H1–N bond is formed. These changes result in migration of H1 from the C atom to the N atom, the products composite NH$_3$ and CO are obtained and are verified by Internal Reaction Coordinate (IRC).

Figure 4. B3LYP/6-31++G (d,p)-optimized structures (in Å) of the stationary points of hydrolysis of HCN with Cu-ZSM5 in the gas phase of path A. The values correspond to the relative free energy (ΔG) in kcal/mol with respect to the separate reactants.

Figure 5. B3LYP/6-31++G (d,p)-optimized structures (in Å) of the stationary points of hydrolysis of HCN with Cu-ZSM5 in the gas phase for path B. The values correspond to the relative free energy (ΔG) in kcal/mol with respect to the separate reactants.

Figure 6. B3LYP/6-31++G (d,p)-optimized structures (in Å) of the stationary points of hydrolysis of HCN with Cu-ZSM5 in the gas phase for path C. The values correspond to the relative free energy (ΔG) in kcal/mol with respect to the separate reactants.
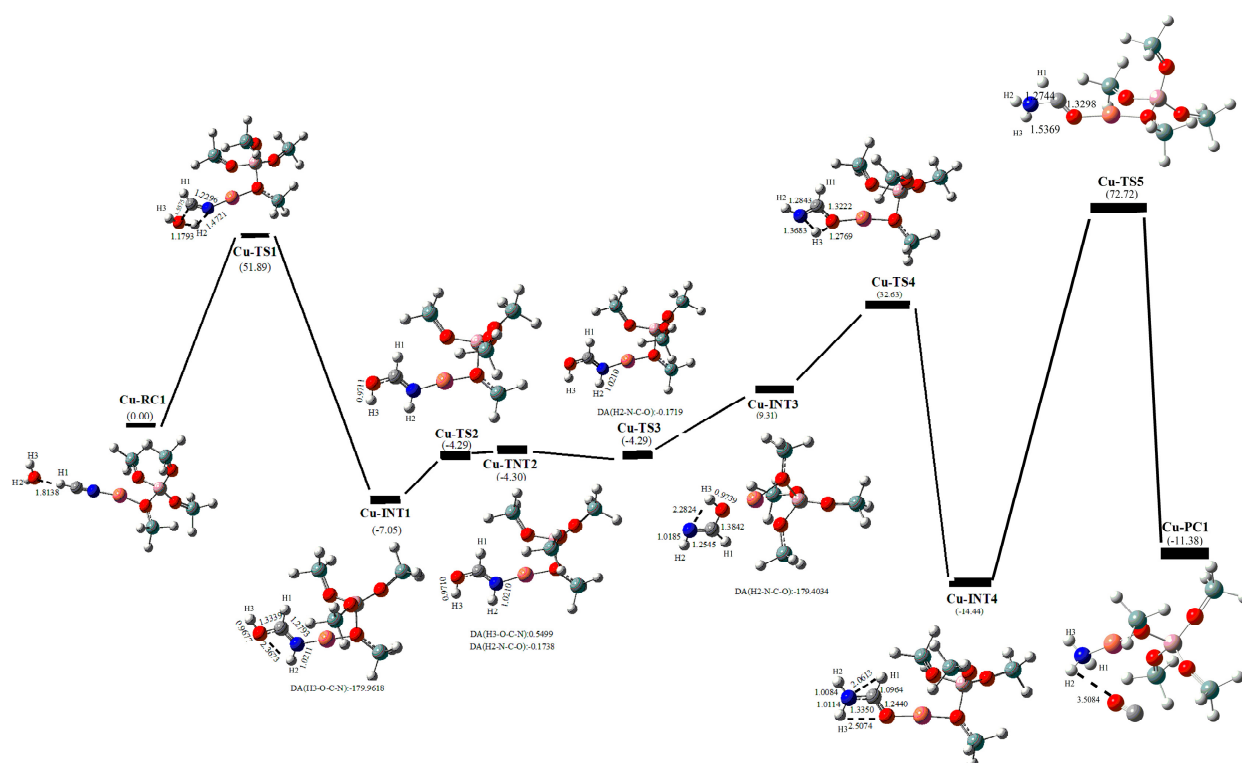

Figure 7. B3LYP/6-31++G (d,p)-optimized structures (in Å) of the stationary points of hydrolysis of HCN with Cu-ZSM5 in the gas phase for the path D. The values correspond to the relative free energy (ΔG) in kcal/mol with respect to the separate reactants.
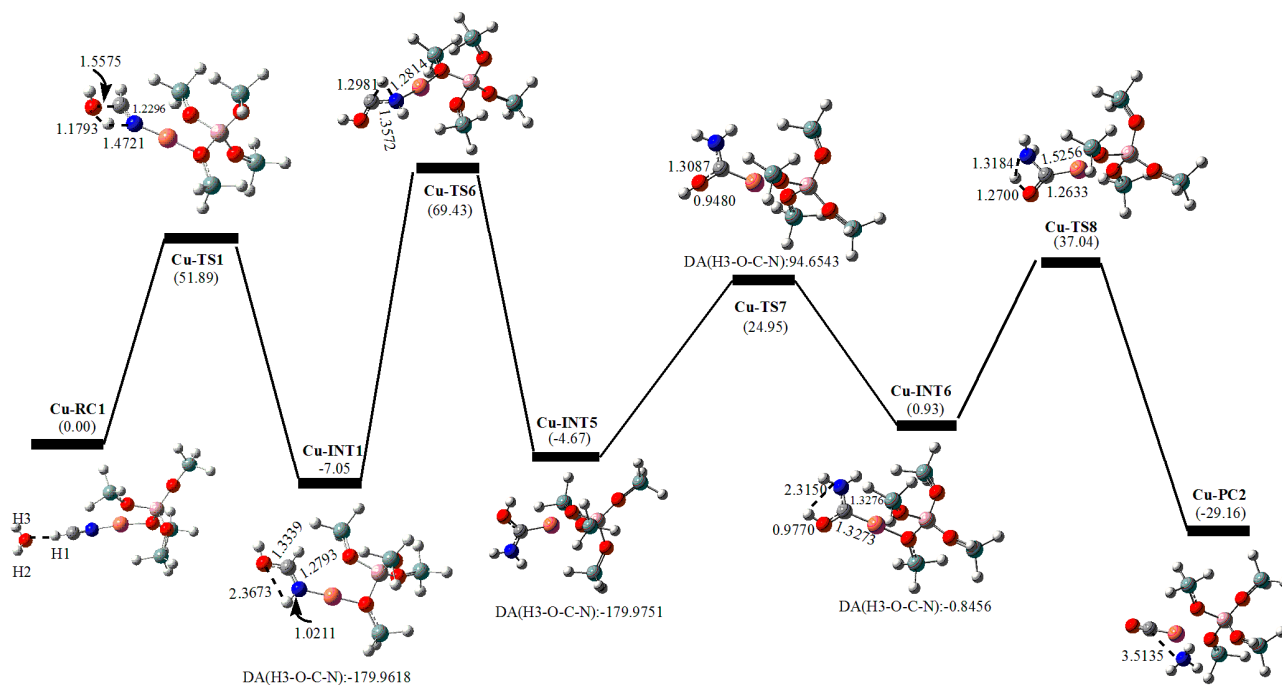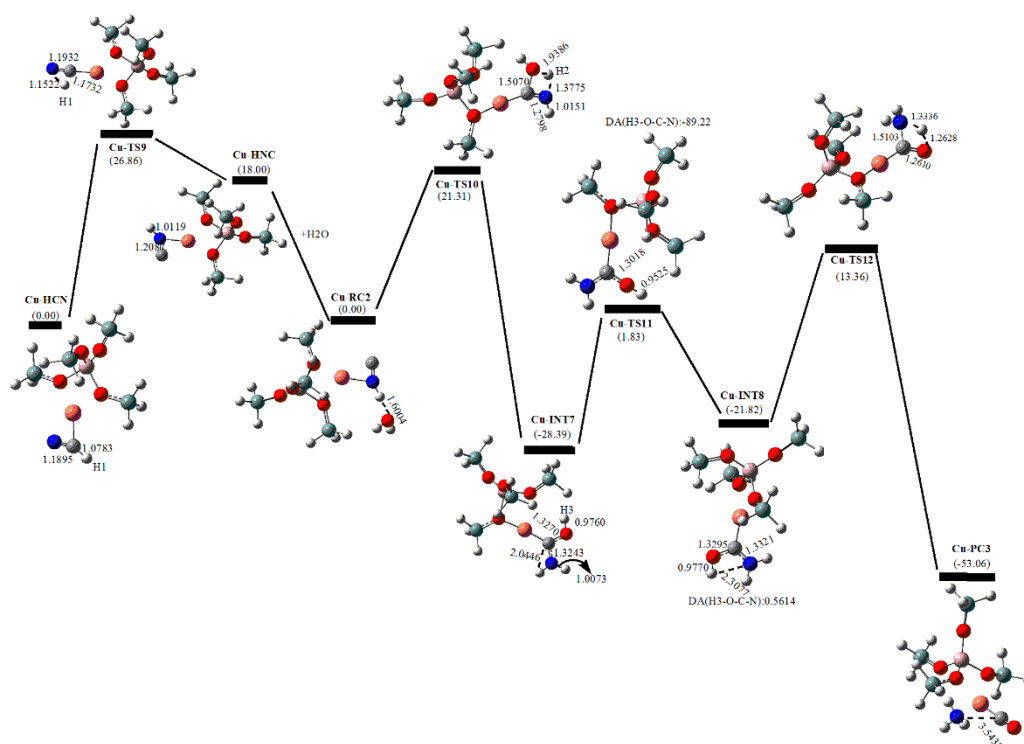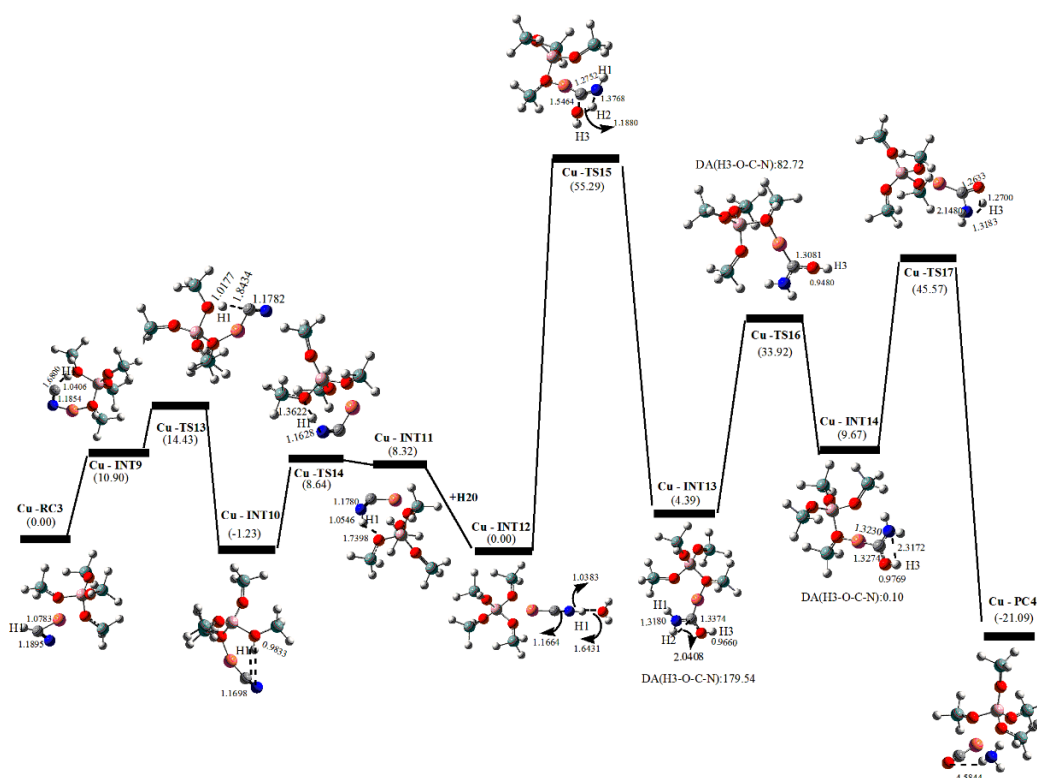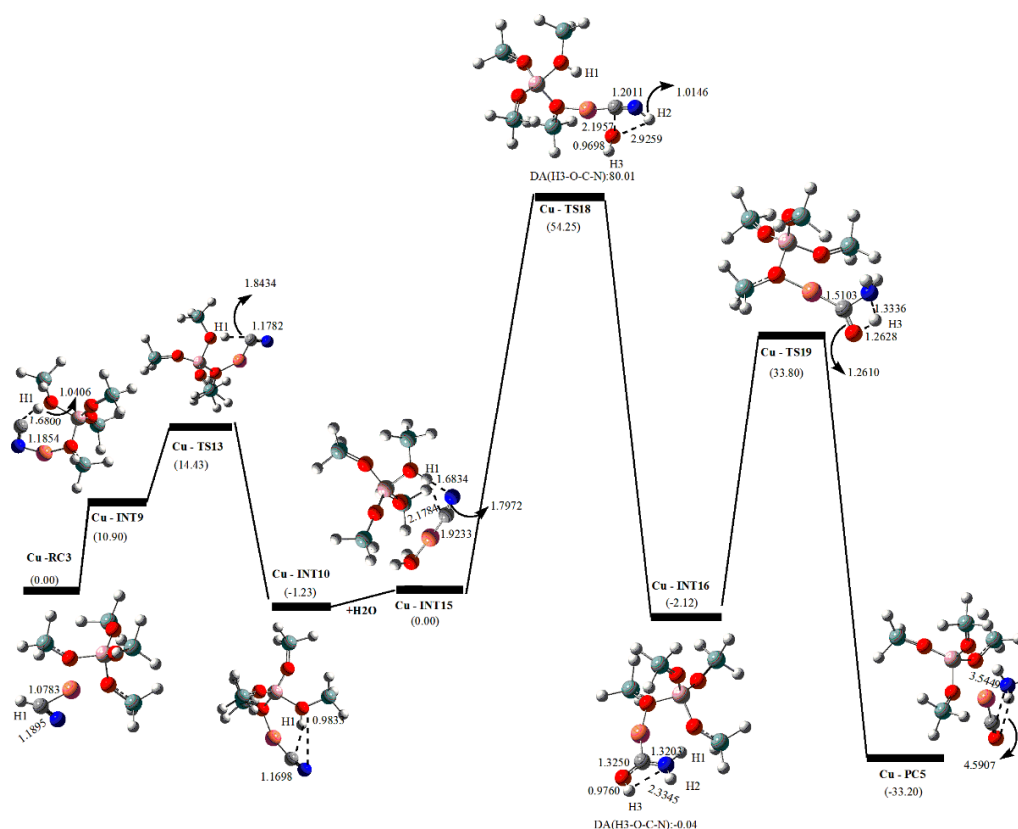
Figure 8. B3LYP/6-31++G (d,p)-optimized structures (in Å) of the stationary points of hydrolysis of HCN with Cu-ZSM5 in the gas phase for the path E. The values correspond to the relative free energy (ΔG) in kcal/mol with respect to the separate reactants.

Table 1 shows the corresponding free energy of the separate reactants with the pathA.The free energy barrier $\Delta G^{\neq}$ of Cu-TS1, Cu-TS2, and Cu-TS3 are 51.89 kcal/mol, 2.76 kcal/mol, and 0.01 kcal/mol, respectively. Notably, Cu-TS1 has the lowest free energy barrier, indicating that when HCN isomerizes to HNC the reaction easily occurred from Cu-NT1 to Cu-INT3. The free energy barrier $\Delta G^{\neq}$ of Cu-TS4 is 23.32 kcal/mol, which is lower comparedto that of the Cu-TS1, but higher compared to those of Cu-TS2 and Cu-TS3. The free barrier $\Delta G^{\neq}$ for Cu-TS5 is 87.15 kcal/mol, and the transfer of H1 atom in Cu-TS5 from C atom to N atom and breaking of the C–N bond take place. These findings show that the last step is the rate-controlling step with a three membered transition state.

3.2. Path B

The first step for path B (Figure 5) is similar to that of path A. In the subsequent steps, proton (H1) from the carbon atom is transferred to the N atom. After the previous intermediate, the Cu-TS6 emerges along the potential energy profile with one imaginary frequency of -1743.80 icm^{-1}. Cu-TS6 contains H1–N and H1–C bonds. This vibrational mode shows that the H1 shifts to the N atom of HCN. In Cu-TS6, the distance between H_2 and N atomic is 1.2814 Å, which longer compares with the distance in Cu-INT1. H1 then moves to the N atom of HCN forming H1–N bond. Concomitantly, Cu-INT5 is formed through Cu-TS6, and the distance from H1 atom to N atom is 3.0098 Å in Cu-INT5.

In the next step, H3 starts to deflect through Cu-INT5, and a transition state Cu-TS7 is formed with an energy barrier of 29.62 kcal/mol. Notably, Cu-TS7 has one imaginary frequency of -1256.75 icm^{-1}. H3 continues to deflect through Cu-TS7, resulting in iso-merization of Cu-TS7 into Cu-INT6 intermediate. The length of H3–O bond in Cu-INT6 is 0.9770 Å, whereas the distance between H3 atom and N atom is 2.3150 Å. To obtain the final products NH$_3$ and CO, the hydrogen atom (H3) of oxygen atom completely shifts to

the nitrogen atom of HCN. The vibrational mode of the single imaginary frequency for the four-membered ring Cu-TS8 is -1694.05 icm^{-1} and it contains H3–O and H1–N bonds. Subsequently, the transition state, Cu-TS8 is overcome by the formation of the product Cu-PC2 (NH_3 + CO). At this step, H3–N bond is formed completely, whereas C–N bond is broken.

Table 1. Relative energies (in kcal/mol) with respect to the reactant complex (RC) for the catalytic hydrolysis of HCN with Cu-ZSM-5 in the gas phase of path A at the B3LYP/6–31++G (d,p) level.

	ΔE_e^a	$T\Delta S_{TRV}^b$	ΔE_0^c	ΔE_{TRV}^d	ΔH^e	ΔG^f	$\Delta G^{\neq g}$
Path A Cu-RC1	0.00	0.00	0.00	0.00	0.00	0.00	
Cu-TS1	51.13	−3.30	49.92	48.60	48.60	51.89	51.89
Cu-INT1	0.00	−4.29	−9.83	−11.34	−11.34	−7.05	
Cu-TS2	−11.74	−5.75	−8.03	−10.04	−1n0.04	−4.29	2.76
Cu-INT2	−11.74	−5.74	−8.03	−10.04	−10.04	−4.30	
Cu-TS3	−11.74	−5.75	−8.03	−10.04	−10.04	−4.29	0.01
Cu-INT3	4.95	−2.87	7.61	6.44	6.44	9.31	
Cu-TS4	31.31	−3.04	30.87	29.59	29.59	32.63	23.32
Cu-INT4	−19.27	−2.91	−16.22	−17.34	−17.35	−14.44	
Cu-TS5	73.62	−2.06	71.55	70.65	70.65	72.72	87.15
Cu-PC1	−11.17	1.24	−10.37	−10.14	−10.14	−11.38	

Abbreviations for the species names are shown in Figures 4–8. ΔE_e corresponds to the electronic energy; ΔE_0 corresponds to zero-point vibration energy; $\Delta ETRV = \Delta E_e$ + vibration energy; ΔH corresponds to the enthalpy; ΔG corresponds to Gibbs free energy; $\Delta G^{\neq}$ corresponds to activation free energy barrier.

The free energy barrier $\Delta G^{\neq}$ of Cu–TS6, Cu-TS7, and Cu-TS8 is 76.13 kcal/mol, 24.95 kcal/mol, and 37.04 kcal/mol, respectively, (Table 2), which are lower comparedto that of the Cu-TS6 step. Cu-TS6 has the highest free energy barrier, implying that the second step is the rate-controlling step. The lowest free energy barrier is the third step in path B, which is the most likely step to occur. Compared with path A, energy barrier of the rate-limiting step of path B is significantlylower.

Table 2. Relative energies (in kcal/mol) with respect to the reactant complex (RC) for the catalytic hydrolysis of HCN with Cu-ZSM-5 in the gas phase of path B at the B3LYP/6–31++G (d,p) level.

	ΔE_e^a	ΔE_0^c	$T\Delta S_{TRV}^b$	ΔE_{TRV}^d	ΔH^e	ΔG^f	$\Delta G^{\neq g}$
Path B Cu-RC1	0.00	0.00	0.00	0.00	0.00	0.00	
Cu-TS1	51.13	49.92	−3.30	48.60	48.60	51.89	51.89
Cu-INT1	−12.96	−9.34	−4.06	−10.76	−10.76	−6.70	
Cu-TS6	67.03	66.45	−4.43	64.99	64.99	69.43	76.13
Cu-INT5	−10.03	−6.55	−3.79	−8.46	−8.46	−4.67	
Cu-TS7	21.75	22.98	−3.48	21.47	21.47	24.95	29.62
Cu-INT6	−4.44	−1.30	−3.65	−2.72	−2.72	0.93	
Cu-TS8	33.56	33.38	−5.72	31.33	31.33	37.04	36.11
Cu-PC2	−32.97	−31.28	−3.59	−32.75	−32.75	−29.16	

3.3. Path C

Cu-HCN is initially isomerizedto Cu-HNC, mainlythrough the migration of H1 atom from C atom to the N atom (Figure 6). The three-membered ring transition state Cu-TS9 corresponds to this process with an imaginary frequency of -1029.77 icm^{-1}. The length of C≡N bond is 1.1895 Å and the free energy in the Cu-HCN state is 0.00 kcal/mol. However, when Cu-HCN is transitioning to the Cu-HNC isomer, the free energy of Cu-HNC is higher (18.00 kcal/mol) compared to that of Cu-HCN, and the C≡N bond length (1.2087 Å) increases.

In the next step, the Cu-RC2, an initial reactant complex, is observed on the free energy profile (Figure 6) after addition of one water molecule. The distance of H1 atom to O atom is 1.6004 Å. After attack of the C atom of HNC by the O atom of the water, the H_2 atom approaches the C atom of HNC, and the transition state, Cu-TS10 with a four-membered ring structure emerged of path C. Cu-TS10 has one imaginary frequency of -1625.63 icm^{-1}. Cu-TS10 corresponds to breaking of O–H_2 bond and formation of C–O and H_2–N bonds. The C–O bond and the H_2–N bond are fully formed, implying that Cu-INT7 is formed through Cu-TS10. The distance of C–O bond and H_2–N bond are 1.3270 Å and 1.3243 Å, respectively, in Cu-TS10. In the subsequent step, H3 deflects through Cu-TS11 so that the H3 atom can be effectively transferred to the N atom. Notably, the vibrational mode of the imaginary frequency for Cu-TS11 is -1654.36 icm^{-1}. After H3 gotcloser to the N atom of HCN, an intermediate Cu-INT8 is observed, and the distance between H3 and N atom becomes smaller. The hydrogen atom (H3) of water shifts to the nitrogen atom to form the final products NH_3 and CO.At this point, Cu-TS12 with a four-membered ring appears in the potential energy profile. The vibrational mode of the single imaginary frequency for Cu-TS12 is -1694.34 icm^{-1}. This shows that the H3 atom migrates from O atom to N atom. The optimized product Cu-PC3 is subsequently formed after the transition state, Cu-TS12. Notably, the distance of the C≡N bond of the products is higher compared to thatof the reactants after introduction of Cu-ZSM-5 catalyst.

Table 3. Relative energies (in kcal/mol) with respect to the reactant complex (RC) for the catalytic hydrolysis of HCN with Cu-ZSM-5 in the gas phase of path C using the B3LYP/6–31++G (d,p)level.

	ΔE_e^a	ΔE_0^c	$T\Delta S_{TRV}^b$	ΔE_{TRV}^d	ΔH^e	ΔG^f	$\Delta G^{\neq g}$
Path C Cu-HCN	0.00	0.00	0.00	0.00	0.00	0.00	
Cu-TS9	30.72	1.21	27.81	28.06	28.06	26.86	26.86
Cu-HNC	15.36	−3.46	14.20	14.54	14.54	18.00	
Cu-RC2	0.00	0.00	0.00	0.00	0.00	0.00	
Cu-TS10	19.47	−3.05	19.76	18.25	18.25	21.31	21.31
Cu-INT7	−33.87	−2.30	−29.35	−30.69	−30.69	−28.39	
Cu-TS11	0.09	−1.16	1.95	0.67	0.67	1.83	30.22
Cu-INT8	−24.86	−0.52	−21.34	−22.33	−22.33	−21.82	
Cu-TS12	12.15	−2.31	12.65	11.32	11.32	13.63	35.45

The free energy barriers of the four steps of path C are 26.86, 21.32, 30.22, and 35.45 kcal/mol, respectively. The highest free energy barrier is the last step, implying that the last step is the rate-controlling step. The free energy barrier of the second step is the lowest in this path, implying that itismore likely to occur comparedto the other steps.

3.4. Path D

The H1 atom migrates from C atom to Cu-ZSM-5 molecular sieve (Figure 7). The transition of Cu-RC3 to Cu-INT9 corresponds to this process. An initial reactant complex (Cu-RC3) appears before the transfer of H1 atom. TheH1–C bond length is 1.1895 Å in Cu-RC3. H1–C bond breaks after the formation of Cu-RC3, and an intermediate Cu-INT9 is formed. The distance between H1 and C is 1.6800 Å for Cu-INT9. Furthermore, in order to form Cu-HNC, H1 shifts to C atom, and the first transition state Cu-TS13emerges along the potential energy profile with one imaginary frequency of -190.66 icm^{-1}. The transition state, Cu-TS13 is the connection between the intermediate Cu-INT9 and Cu-INT10. The free energy of Cu-TS13 is 14.43 kcal/mol. An intermediate Cu-INT10 is observedafter the transition state Cu-TS13. The distance between H1atom and O atom on the Cu-ZSM-5 decreases from 1.0406 Å to 0.9833 Å from intermediate Cu-INT9 to Cu-INT10. After the formation of Cu-INT10, the transition state Cu-TS14 appears with one imaginary frequency of -277.05 icm^{-1}. This vibrational mode indicates that H1 atom gets close to the N atom. The length of C≡N and H1–O bonds in Cu-TS14 is longer comparedto those of Cu-INT10,

whereas the length of H1–N bond (1.1628Å) is shorter comparedto that of Cu-INT10. These changes indicate that H1 is far from the O atom in Cu-ZSM-5 and gradually approaches the N atom in HCN. Concomitantly, the second intermediate Cu-INT11 appears with the formation of Cu-HNC.The distance between H1atom and N atom in Cu-INT11 is 1.0546 Å.

After the formation of Cu-HNC, one water molecule is added to attract HNC, resulting in an initial reaction complex, Cu-INT12. The lengths between C–N and H1–N bonds are 1.1664 Å and 1.6431 Å in Cu-INT12. A four-membered ring transition state Cu-TS15 appears along the potential energy profile when the H_2 atom of H_2O gets closer to the N atom. The vibrational mode of the single imaginary frequency is -1591.27 icm^{-1}, corresponding to the breaking of O–H_2 bond. The H_2–O atomic distance is 1.1880 Å in Cu-TS15, and the relative free energy barrier of Cu-TS15 is 55.29 kcal/mol. Then H_2 completely transfers to N, resulting in the formation of C–O and N–H_2 bonds. In this step, the Cu-INT13 intermediate is formed. The dihedral angle (H3–O–C–N) (DA) of Cu-INT13 is 179.54°, and the subsequent step corresponds to the twisting of H3 on O atom. The transition state Cu-TS16 appears after Cu-INT13. The single imaginary frequency in Cu-TS16 is -1256.66 icm^{-1} with a free energy barrier of 33.92 kcal/mol. The H3 on O continues to twist, resulting in the elongation of O–H bond and shortening of N–H bond. Transfer of H3 on O allows the H3 atom to fit and interact with the N atom. The intermediate Cu-INT14 is thenformed, resulting in the elongation of O–H bond and shortening of N–H bond. The dihedral angle (H3–O–C–N) (DA) is 0.0984° in Cu-INT14. Subsequently, H3 atom is transferred to the N atom of HCN to form the finalproduct complex (NH_3 +CO). A four-member ring transition state (Cu-TS17) is formed through Cu-INT14. The vibrational mode of the single imaginary frequency for Cu-TS17is -1694.06 icm^{-1}, and the free energy barrier is 45.57 kcal/mol. O–H3 bond is completely broken, and the distance between the N atom and H3 atom is decreased by approximately 1.0000 Å during the transition from Cu-INT14 to Cu-TS17. Notably, H3 approaches the N atom. After overcoming the transition state, the target product complex Cu-PC4 (CO and NH_3) is formed. The free energy barrier of Cu-PC4 is -21.09 kcal/mol, meaning thatchange from the transition state Cu-TS17 to the final product complex Cu-PC4 is an exothermic process.

The free energy barrier $\Delta G^{\neq}$ for the five steps is 14.43, 9.88, 55.29, 29.53, and 35.90 kcal/mol, respectively (Table 4). The free energy barriers show that the free energy barrier of third step is the highest, therefore, the rate-determiningstep in path D is Cu-INT12$\rightarrow$ Cu-TS1$\rightarrow$Cu-INT13, which is more hardly to occur compared with the other steps.

Table 4. Relative energies (in kcal/mol) with respect to the reactant complex (RC) for the catalytic hydrolysis of HCN with Cu-ZSM-5 in the gas phase of path D at the B3LYP/6–31++G (d,p) level.

	ΔE_e^a	$T\Delta S_{TRV}^b$	ΔE_0^c	ΔE_{TRV}^d	ΔH^e	ΔG^f	$\Delta G^{\neq g}$
Cu-RC3	0.00 6	0.00	0.00	0.00	0.00	0.00	
Cu-INT9	11.62	0.44	11.20	11.33	11.33	10.90	
Cu-TS13	15.49	0.58	15.11	15.01	15.01	14.43	14.43
Cu-INT10	−1.54	0.65	−0.64	−0.58	−0.58	−1.23	
Cu-TS14	10.74	−0.53	8.41	8.11	8.11	8.64	9.88
Cu-INT11	10.53	1.52	9.55	9.84	9.84	8.32	
Cu-INT12	0.00	0.00	0.00	0.00	0.00	0.00	
Cu-TS15	50.76	−6.63	50.28	48.66	48.66	55.29	55.29
Cu-INT13	−4.94	−6.89	−0.81	−2.50	−2.50	4.39	
Cu-TS16	27.10	−6.85	28.84	27.07	27.07	33.92	29.53
Cu-INT14	0.90	−6.77	4.56	2.90	2.90	9.67	
Cu-TS17	39.87	−7.98	39.69	37.58	37.58	45.57	35.90
Cu-PC4	−28.50	−5.95	−26.07	−27.04	−27.04	−21.09	

3.5. Path E

Similar to the path D, the first step of path E is transfer of H atom from HCN to Cu-ZSM-5 (Figure 8), and transitionfrom Cu-RC3 to Cu-INT10 is included in this process.

In the subsequent step, one water molecule is introduced, and an initial reaction complex Cu-INT15 is formed. H_2 atom on the H_2O moves to the N atom, and a four-membered ring transition state Cu-TS18 is formed. The only imaginary frequency of Cu-TS18 is -202.08 icm^{-1}. The vibration model indicates preferential cleavage of $O–H_2$ bond and formation of $N–H_2$ bond. The distance between O atom and H_2 atom is 2.9259 Å, and the free energy barrier $\Delta G^{\neq}$ for Cu-TS18 is 54.25kcal/mol with respect to the separate reactants. The free energy barrier $\Delta G^{\neq}$ is highest in this step (Table 5). This indicates that this step presents the highest energy, therefore it is the rate-limiting step. The next step is transfer of H1 on Cu-ZSM-5 to N atom, on the basis of the transition state Cu-TS18. H1 atom gradually approached the N atom. In this step, the H3 atom on O atom is twisted simultaneously, with the dihedral angle (H_3–O–C–N)(DA) twisting to $-0.04°$, and N–H1 and C–O bonds are formed. These changes result in the formation of a four-membered ring intermediate (Cu-INT16). The distance between N atom and H3 atom is 2.3345 Å, and the length of H3–C bond in Cu- INT16is 0.9760 Å.

To ensure that H_3 atom is successfully transferred to the N atom, the H_3 atom on N atom should change the position. Subsequently, H3 slowly approaches the N atom. Decrease inthe distance between the H3 atom and the N atomof Cu-INT16 from 2.3345 Å to 1.3336 Å, results in the formation of a four-membered ring transition state Cu-TS19. The only imaginary frequency of Cu-TS19 is -1694.35icm^{-1}. The vibration model corresponds to the cleavage of the $O–H_3$ bond and formation of $N–H_3$ bond. The free energy barrier $\Delta G^{\neq}$ of Cu-TS19 is 33.80 kcal/mol. After the transition state Cu-TS19 is overcome, the finalproduct complex Cu-PC5 is formed. In this step, H3–N bond is formed, and H3–O bond is completely broken. The virtual length of N–C bond in Cu-PC5 is 3.5449 Å, which is approximately 2.3000 Å longer comparedto that of Cu-INT16. This indicates that the degree of bond formation is greater comparedto the degree of bond cleavage in this catalytic hydrolysis reaction.

The free energy barriers of path E are listed in Table 5. The free energy barriers of the first step, second step, and third step are 14.43 kcal/mol, 54.25 kcal/mol, and 35.29 kcal/mol, respectively. These findings show that the second step is the rate-controlling step. The first step corresponds to transfer of H atom on HCN, and has the lowest free energy barrier (14.43 kcal/mol). This indicates that the first step is the most likely step to occur in path E.

Table 5. Relative energies (in kcal/mol) with respect to the reactant complex (RC) for the catalytic hydrolysis of HCN with Cu-ZSM-5 in the gas phase of path E at the B3LYP/6–31++G (d,p) level.

	ΔE_e^a	ΔE_0^c	$T\Delta S_{TRV}^b$	ΔE_{TRV}^d	ΔH^e	ΔG^f	$\Delta G^{\neq g}$
Path E Cu-RC3	0.00	0.00	0.00	0.00	0.00	0.00	
Cu-INT9	11.62	0.44	11.20	11.33	11.33	10.90	
Cu-TS13	15.49	0.58	15.11	15.01	15.01	14.43	14.43
Cu-INT10	−1.54	0.65	−0.64	−0.58	−0.58	−1.23	
Cu-INT15	0.00	0.00	0.00	0.00	0.00	0.00	
Cu-TS18	68.90	0.16	54.59	54.41	54.41	54.25	54.25
Cu-INT16	−4.46	−0.54	−1.97	−2.66	−2.66	−2.12	
Cu-TS19	35.09	−0.59	33.88	33.21	33.21	33.80	35.92
Cu-PC5	−33.27	1.21	−32.11	−31.99	−31.99	−33.20	

4. Conclusions

In this study, five catalytic hydrolysis pathways (paths A, B, C, D, and E) of HCN were explored using the B3LYP method. The free energy barriers and activation energy barrier are the lowest in path C compared to the othercatalytic hydrolysis pathways. These findings show that the kinetically favorable mechanism involves isomerization of HCN to HNC. Findings from our previous studyshow that the presence of catalystCu-ZSM-5 could significantly reduce the energy barrier of HCN isomerization to HNC, thus

improving effectiveness of the entire pathway. This is of great theoretical and practical significance in guiding development of a novel high efficiency catalytic system for HCN catalytic hydrolysis and simplifying the experimental process of HCN hydrolysis which has high toxicity.

Author Contributions: Conceptualization, Y.Z. and F.L.; methodology, Y.Z.; software, F.L.; validation, Y.Z., F.L. and C.Y.; formal analysis, C.Y.; investigation, F.L.; resources, C.Y.; data curation, G.P.; writing—original draft preparation, G.P.; writing—review and editing, G.W.; visualization, F.X.; supervision, F.X.; project administration, F.X.; funding acquisition, F.X. All authors have read and agreed to the published version of the manuscript.

Data Availability Statement: Not available.

Conflicts of Interest: The authors declare no conflict of interest.

References

1. Wang, Z.; Jiang, M.; Ning, P.; Xie, G. Thermodynamic modeling and gaseous pollutionprediction of the yellow phosphorus production. *Ind. Eng. Chem. Res.* **2011**, *50*, 12194–12202. [CrossRef]
2. Zhao, Q.; Tian, S.; Yan, L.; Zhang, Q.; Ning, P. Novel HCN sorbents based on layered double hydroxides: Sorption mechanism and performance. *J. Hazard. Mater.* **2015**, *285*, 250–258. [CrossRef] [PubMed]
3. Sing, K.S.W. Reporting physisorption data for gas/Solid systems-with Special Reference to the Determination of Surface Area and Porosity. *Pure Appl. Chem.* **1985**, *57*, 603–619. [CrossRef]
4. Yang, Y.; Suh, S. Environmental impacts of products in China. *Environ. Sci. Technol.* **2011**, *45*, 4102–4109. [CrossRef] [PubMed]
5. Jiang, M.; Wang, Z.H.; Ning, P.; Tian, S.L.; Huang, X.F.; Bai, Y.W.; Shi, Y.; Ren, X.G.; Chen, W.; Qin, Y.S.; et al. Dust removal and purificationofcalcium carbide furnace off-gas. *Environ. Sci. Technol.* **2014**, *45*, 901–907.
6. Ma, J.; Dasgupta, P.K. Recent developments in cyanide detection: A review. *Anal. Chim. Acta* **2010**, *673*, 117–125. [CrossRef]
7. Tang, Y.; Chen, W.; Li, C.; Pan, L.; Dai, X.; Ma, D. Adsorption behavior of Co anchored on graphene sheets toward NO, SO$_2$, NH$_3$, CO and HCN molecules. *Appl. Surf. Sci.* **2015**, *342*, 191–199. [CrossRef]
8. Liu, J.H.; Lv, C.Q.; Guo, Y.; Wang, G.C. Theoretical study of the adsorption and dissociation mechanism for methylamine on Pd(111). *Appl. Surf. Sci.* **2013**, *271*, 291–298. [CrossRef]
9. Hu, Y.; Liu, J.; Cheng, J.; Wang, L.; Tao, L.; Wang, Q.; Wang, X.; Ning, P. Coupling catalytic hydrolysissand oxidation of HCN over HZSM-5 modified by metal (Fe, Cu) oxides. *Appl. Surf. Sci.* **2018**, *427*, 843–850. [CrossRef]
10. Kröcher, O.; Elsener, M. Hydrolysissand oxidation of gaseous HCN over heterogeneous catalysts. *Appl. Catal. B* **2009**, *92*, 85–89. [CrossRef]
11. Wang, L.; Wang, X.; Jing, X.; Ning, P. Efficient removal of HCN through catalytic hydrolysissand oxidation on Cu/CoSPc/Ce metal-modified activated carbon under low oxygen conditions. *RSC Adv.* **2016**, *6*, 113834–113843. [CrossRef]
12. Giménez-López, J.; Millera, A.; Bilbao, R.; Alzueta, M.U. HCN oxidation in an O$_2$/CO$_2$, atmosphere: An experimental and kinetic modeling study. *Combust. Flame* **2010**, *157*, 267–276. [CrossRef]
13. Marsh, J.D.F.; Newling, W.B.S.; Rich, J. The catalytic hydrolysissof hydrogen cyanide to ammonia. *J. Chem. Technol. Biotechnol.* **2010**, *2*, 681–684.
14. Nanba, T.; Obuchi, A.; Akaratiwa, S.; Liu, S.; Uchisawa, J.; Kushiyama, S. Catalytic hydrolysissof HCN over H-Ferrierite. *Chem. Lett.* **2000**, *2000*, 986–987. [CrossRef]
15. Wang, L.; Wang, X.; Cheng, J.; Ning, P.; Lin, Y. Coupling catalytic hydrolysissand oxidation on Mn/TiO$_2$-Al$_2$O$_3$ for HCN removal. *Appl. Surf. Sci.* **2018**, *439*, 213–221. [CrossRef]
16. Jensen, J.O.; Krishnan, P.N.; Burke, L.A. Theoretical study of possible products of the combination of H$_2$O and HCN. *J. Mol. Struct.* **1996**, *370*, 245–252. [CrossRef]
17. Li, J.; Han, K.L.; He, G.Z. Computational study on the addition of HCN to methanimine catalyzed by formamidine and formamide. *J. Mol. Struc. Theochem.* **2005**, *713*, 51–57. [CrossRef]
18. Koch, D.M.; Toubin, C.; Xu, S.; Peslherbe, G.H.; Hynes, J.T. Concerted proton-transfer mechanism and solvation effects in the HNC/HCN isomerization on the surface of icy grain mantles in the interstellar medium. *J. Phys. Chem. C* **2007**, *111*, 15026–15033. [CrossRef]
19. Basharnavaz, H.; Habibi-Yangjeh, A.; Mousavi, M. Ni, Pd, and Pt-embedded graphitic carbon nitrides as excellent adsorbents for HCN removal: A DFT study. *Appl. Surf. Sci.* **2018**, *456*, 882–889. [CrossRef]
20. Song, X.; Ning, P.; Li, K.; Sun, X.; Wang, C.; Sun, L. Hydrogen transfer effect and reaction mechanism for catalytic hydrolysiss of HCN in ionic liquids: A density functional theory study. *Chem. Eng. J.* **2018**, *348*, 630–636. [CrossRef]

21. Kachurovskaya, N.A.; Zhidomirov, G.M.; Hensen, E.J.; van Santen, R.A. Cluster model DFT study of the intermediates of benzene to phenol oxidation by N_2O on FeZSM-5 zeolites. *Catal. Lett.* **2003**, *86*, 25–31. [CrossRef]

22. Zhang, B.; He, G.; Shan, Y.; He, H. Experimental and DFT study of the adsorption of N_2O on transition ion-exchanged ZSM-5. *Catal. Today* **2019**, *327*, 177–181. [CrossRef]

23. Li, G.; Pidko, E.A.; van Santen, R.A.; Feng, Z.; Li, C.; Hensen, E.J. Stability and reactivity of active sites for direct benzene oxidation to phenol in Fe/ZSM-5: A comprehensive periodic DFT study. *J. Catal.* **2011**, *284*, 194–206. [CrossRef]

24. Czekaj, I.; Brandenberger, S.; Kröcher, O. Theoretical studies of HNCO adsorption at stabilized iron complexes in the ZSM-5 framework. *Micropor. Mesopor. Mat.* **2013**, *169*, 97–102. [CrossRef]

25. Xia, F.; Ning, P.; Zhang, Q.; Li, F.; Tao, G.; Tian, K.; Huang, X.; Peng, J.; Zhu, H. A gas-phase ab initio study of the hydrolysiss of HCN. *Theor. Chem. Acc.* **2016**, *135*, 1–14. [CrossRef]

26. Kuharski, R.A.; Rossky, P.J. A quantum-mechanical study of structure in liquid H_2O and D_2O. *J. Chem. Phys.* **1985**, *82*, 5164–5177. [CrossRef]

27. Balucani, N.; Asvany, O.; Chang, A.H.H.; Lin, S.H.; Lee, Y.T.; Kaiser, R.I.; Osamura, Y. Crossed beam reaction of cyano radicals with hydrocarbon molecules. III. Chemical dynamics of vinylcyanide (CHCN;XA) formation from reaction of CN(X) with ethylene, CH(X1Ag). *J. Chem. Phys.* **2000**, *113*, 8643. [CrossRef]

28. Baboul, A.G.; Curtiss, L.A.; Redfern, P.C.; Raghavachari, K. Gaussian-3 theory using density functional geometries and zero-point energies. *J. Chem. Phys.* **1999**, *110*, 7650–7657. [CrossRef]

29. Gonzalez, C.; Schlegel, H.B. An improved algorithm for reaction path following. *J. Chem. Phys.* **1989**, *90*, 2154–2161. [CrossRef]